LASER INTERFEROMETER GRAVITATIONAL WAVE OBSERVATORY
- LIGO -
CALIFORNIA INSTITUTE OF TECHNOLOGY
MASSACHUSETTS INSTITUTE OF TECHNOLOGY

Publication **LIGO-P980007-00 – D** 10/23/98

Gravitational Waves

Daniel Sigg
LIGO Hanford Observatory, P.O. Box 1970 S9-02,
Richland, WA 99352

to be published in the

Proceedings of TASI 98
(Theoretical Advanced Study Institute in Elementary Particle Physics)

Boulder, Colorado

California Institute of Technology
LIGO Project - MS 51-33
Pasadena CA 91125
Phone (626) 395-2129
Fax (626) 304-9834
E-mail: info@ligo.caltech.edu

Massachusetts Institute of Technology
LIGO Project - MS 20B-145
Cambridge, MA 01239
Phone (617) 253-4824
Fax (617) 253-7014
E-mail: info@ligo.mit.edu

WWW: http://www.ligo.caltech.edu/

GRAVITATIONAL WAVES

DANIEL SIGG
LIGO Hanford Observatory, P.O. Box 1970 S9-02,
Richland, WA 99352, USA
E-mail: sigg_d@ligo.mit.edu

A new generation of long baseline gravitational wave detectors is currently under construction (LIGO, VIRGO, GEO and TAMA). They incorporate high sensitive Michelson interferometers and have a design goal of measuring displacements of order 10^{-17} m r.m.s., integrated over a 100 Hz bandwidth centered at the minimum noise region. The purposes of these detectors is to observe gravitational waves from astrophysical sources at cosmological distances, and to open a new view to the universe by collecting information not accessible by conventional telescopes. These lectures present a description of the most promising candidate sources; and summarize the design characteristics of interferometric detectors—in particular, the Laser Interferometer Gravitational-wave Observatory (LIGO).

1 Introduction

According to general relativity theory gravity can be expressed as a space-time curvature[1,2]. One of the theory predictions is that a changing mass distribution can create ripples in space-time which propagate away from the source at the speed of light. These freely propagating ripples in space-time are called gravitational waves. Any attempts to directly detect gravitational waves have not been successful yet. However, their indirect influence has been measured in the binary neutron star system PSR1913+16[3,4,5,6].

This system consist of two neutron stars orbiting each other. One of the neutron stars is active and can be observed as a radio pulsar from earth. Since the observed radio pulses are Doppler shifted by the orbital velocity, the orbital period and its change over time can be determined precisely. If the system behaves according to general relativity theory, it will loose energy through the emission of gravitational waves. As a consequence the two neutron stars will decrease their separation and, thus, orbiting around each other at a higher frequency. From the observed orbital parameters one can first compute the amount of emitted gravitational waves and then the inspiral rate. The calculated and the observed inspiral rates agree within experimental errors (better than 1%).

Gravitational waves are quite different from electro-magnetic waves. Most electro-magnetic waves originate from excited atoms and molecules, whereas observable gravitational waves are emitted by accelerated massive objects.

Also, electro-magnetic waves are easily scattered and absorbed by dust clouds between the object and the observer, whereas gravitational waves will pass through them almost unaffected. This gives rise to the expectation that the detection of gravitational waves will reveal a new and different view of the universe. In particular, it might lead to new insights in strong field gravity by observing black hole signatures, large scale nuclear matter (neutron stars) and the inner processes of supernova explosions. Of course, stepping into "uncharted territory" also carries the possibility to encounter the unexpected and to discover new kinds of astrophysical objects.

Table 1 shows an overview of the gravitational wave frequency bands, their most mature detection methods and their most likely sources.

Currently, a number of long baseline laser interferometers are under construction with the goal to be operational at the beginning of the new millennium. These interferometers incorporate high power stabilized laser sources, complicated optical configurations, suspended optical components and high performance seismic filters. They have arm lengths of up to 4 km and operate in a ultra high vacuum environment.

Table 1. Overview of frequency bands, detection methods and sources (see Ref.[7], and references therein). NS – neutron star and BH – black hole.

f(Hz)	λ	**method**	**source**
$\sim 10^{-16}$	$\sim 10^9$ lt.yrs.	anisotropy of μwave background	primordial
$\sim 10^{-9}$	~ 10 lt.yrs.	timing of milli second pulsars	primordial, cosmic strings
$\sim 10^{-4}$ to 10^{-1}	~ 0.01 AU to 10 AU	Doppler tracking of spacecraft, laser interferometer in space (LISA)	binary stars, supermassive black holes
~ 10 to 10^3	~ 300 km to $30,000$	laser interferometers on earth (VIRGO, LIGO, GEO, TAMA)	inspirals: NS/NS, NS/BH, BH/BH
$\sim 10^3$	~ 300 km	Cryogenic resonant bar detectors	supernovæ spinning NS

Section 2 introduces gravitational waves and their general relativistic description; section 3 presents a summary of promising astrophysical sources which could be strong enough for a first direct detection. Section 4 describes laser interferometers and, in particular, the Laser Interferometer Gravitational-wave Observatory (LIGO) Project.

2 Waves in General Relativity

2.1 Weak field approximation

General Relativity predicts gravitational waves as freely propagating 'ripples' in space-time[1,2]. Far away from the source one can use the weak field approximation to express the curvature tensor $g_{\mu\nu}$ as a small perturbation $h_{\mu\nu}$ of the Minkowski metric $\eta_{\mu\nu}$ (see, for example, Ref.[8]):

$$g_{\mu\nu} = \eta_{\mu\nu} + h_{\mu\nu} \qquad \text{with } |h_{\mu\nu}| \ll 1 \tag{1}$$

Using this ansatz to solve the Einstein field equations in vacuum yields a normal wave equation. Using the transverse-traceless gauge its general solutions can be written as

$$h_{\mu\nu} = h_+(t - z/c) + h_\times(t - z/c) \tag{2}$$

where z is the direction of propagation and h_+ and $h_\times$ are the two polarizations (pronounced 'plus' and 'cross'):

$$h_+(t - z/c) + h_\times(t - z/c) = \begin{pmatrix} 0 & 0 & 0 & 0 \\ 0 & h_+ & h_\times & 0 \\ 0 & -h_\times & h_+ & 0 \\ 0 & 0 & 0 & 0 \end{pmatrix} e^{(i\omega t - ikx)} \tag{3}$$

The above solution describes a quadrupole wave and has a particular simple physical interpretation (see Fig. 1): Let's assume two free masses are placed at positions x_1 and x_2 ($y = 0$) and a gravitational wave with + polarization is propagating along the z-axis, then the free masses will stay fixed at their coordinate positions, but the space in between—and therefore the distance between x_1 and x_2—will expand and shrink at the frequency of the gravitational wave. Similarly, along the y-axis the separation of two points will decrease and increase with opposite sign. The strength of a gravitational wave is then best expressed as a dimension-less quantity, the strain h which measures the relative length change $\Delta L/L$.

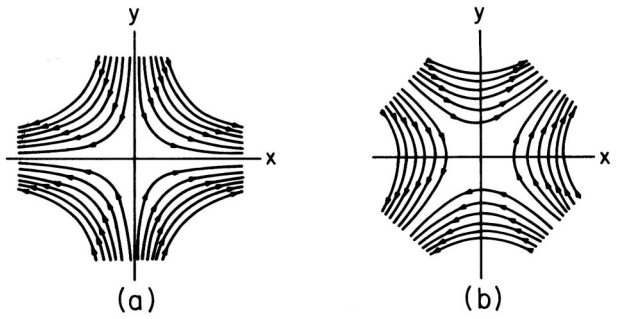

Figure 1. Direction of space deformation for a gravitational wave propagating along the z-axis, + polarization (a) and $\times$ polarization (b).

Table 2 shows a comparison between gravitational wave and electro-magnetic waves[9]. The combination of measuring the amplitude of a gravitational wave and having a large solid angle acceptance makes the event rate of gravi-

Table 2. Comparison between electro-magnetic and gravitational waves[9].

	electro-magnetic waves	**gravitational waves**
medium	space as medium	space-time itself
source	incoherent superposition of atoms and molecules	coherent motion of huge masses
resolution	imaging – λ small compared to source	$\lambda \geq$ scale of sources no spatial resolution
interaction	absorbed, scattered and dispersed by matter	very small interaction no shielding
frequency	10^7 Hz and up	10^4 Hz and down
detection	measure power (light) and amplitude (radio)	measure amplitude
acceptance	detectors are directional	detectors accept large solid angles

tational wave detectors scale with the third power of their sensitivity. In other words, every improvement of a factor of 2 in sensitivity will increase the event rate of astrophysical sources by a factor of 8.

Electro-magnetic waves which are visible to an observer on earth are usually produced in the outer layers of an astrophysical object, whereas gravitational waves carry information about the inside behaviour and the mass distribution of an object. Arguably, the information obtained by the two will be quite different; and it is difficult to predict gravitational sources from electro-magnetic observations.

2.2 Gravitational wave amplitudes

Before looking at possible detection techniques we (very) roughly estimate how large the observed effect of a gravitational wave form an astrophysical source could be. If we denote the quadrupole of the mass distribution of a source by Q, a dimensional argument—together with the assumption that gravitational radiation couples to the quadrupole moment only—yields:

$$h \sim \frac{G\ddot{Q}}{c^4 r} \sim \frac{G(E_{\mathrm{kin}}^{\mathrm{non-symm.}}/c^2)}{c^2 r} \tag{4}$$

with G the gravitational constant and $E_{\mathrm{kin}}^{\mathrm{non-symm.}}$ the non symmetric part of the kinetic energy. If one sets the non-symmetric kinetic energy equal to one solar mass

$$E_{\mathrm{kin}}^{\mathrm{non-symm.}}/c^2 \sim M_\odot \tag{5}$$

and if one assumes the source is located at inter-galactic or cosmological distance, respectively, one obtains a strain estimate of order

$$h \lesssim 10^{-21} \qquad \text{Virgo cluster} \tag{6}$$

$$h \lesssim 10^{-23} \qquad \text{Hubble distance} \tag{7}$$

By using a detector with a baseline of 10^4 m the relative length changes become of order:

$$\Delta L = hL \lesssim 10^{-19}\,\mathrm{m} \text{ to } 10^{-17}\,\mathrm{m} \tag{8}$$

This is a rather optimistic estimate. Most sources will radiate significantly less energy in gravitational waves. We add that the observable effect is not small because the radiated energy is small—in contrary it is huge—but rather because space-time is a "stiff medium".

2.3 Gravitational wave frequencies

Similarly, one can estimate the upper bound for the frequencies of gravitational waves. A gravitational wave source can not be much smaller than its Schwarzshild radius $2GM/c^2$, and cannot emit strongly at periods shorter than the light travel time $4\pi GM/c^3$ around its circumference. This yields a maximum frequency of

$$f \leq \frac{c^3}{4\pi GM} \sim 10^4 \text{ Hz } \frac{M_\odot}{M} \tag{9}$$

From the above equation one can see that the expected frequencies of emitted gravitational waves is the highest for massive compact objects, such as neutron stars or solar mass black holes.

2.4 Experimental evidence for gravitational waves

The only experimental evidence for gravitational waves comes from the timing of binary pulsar systems[6,10]. These systems consists of two neutron stars orbiting each other. To be observable one of them must be active and emit radio waves. Since pulsars emit radio waves mainly along their magnetic axis and since their rotation axis doesn't have to be aligned with the magnetic axis, earth-based radio antennæ can observe a periodic radio signal if the system is aligned so that the radio beacon passes over the earth. The frequency of this signal is determined by the rotation period of the pulsar and is typically of very high precision.

In a double neutron star system this periodic signal is modulated by the orbital frequency of the two neutron stars and can therefore be used to precisely determine the orbital period and phase. The first double pulsar system, PSR B1913+16, was discovered by Hulse and Taylor in 1974[3,4,5]. It is located in the Milky Way, its orbital period is ~ 8 hours and the received radio signal repeats itself at a rate of ~ 17/sec. The emission of gravitational waves brings the two neutron stars closer together, and thus increase the orbital frequency. Fig. 2 shows the advance of the orbital phase as function of time relative to a system which would have a constant orbital period. The loss of potential energy in this system is in agreement with the emission of gravitational waves predicted by general relativity theory[10,11]. As a consequence the two neutron stars will merge in about 300 million years.

Due to their tiny effect on space-time the direct observation of gravitational waves has not been successful until now. A list of the most mature methods, their applicable frequency band and the most likely sources in this band were already presented in Table 1.

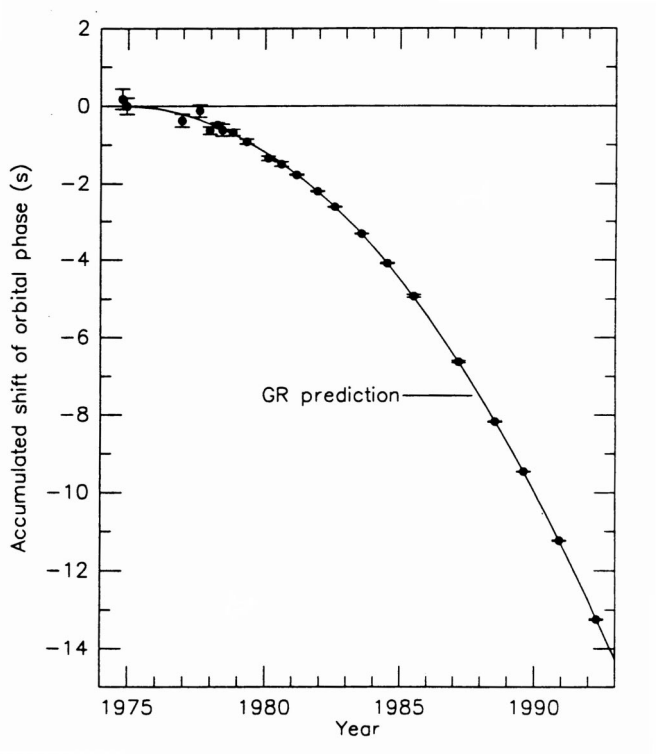

Figure 2. Advance of the orbital phase in the binary pulsar system PSR B1913+16. The plot is taken from Ref.[10].

3 Astrophysical sources

Only massive astrophysical object are good candidates for emitting gravitational waves which can be detected by an observer on earth. A more extensive overview of promising sources of gravitational waves can be found in Ref.[7]; we only give a brief summary here.

3.1 Coalescing compact binaries

Compact binaries are among the best candidates to be first seen by an earth-based gravitational-wave antenna. Compact binaries can consist of either two neutron stars, two black holes or one of each. Due to their small size

($\sim$ 20 km in case of a neutron star), they can orbit each other at close range and a high orbital frequency (up to $\sim$ 500 Hz). Being very close and rotating fast means that the second time derivative of the mass quadrupole moment is large and, hence, gravitational waves are emitted with a high efficiency. Indeed, the radiated energy is so large, that a double neutron star system which is 500 km or 100 km apart will loose all its potential energy within a couple of minutes or seconds, respectively. Since the emission of gravitational wave becomes more efficient at closer range, the waveform is a chirp signal (see Fig. 3 and Ref.[12]): increasing both in amplitude and frequency with time, until the two object are close enough to merge. To first order the the chirp signal can be described by the change of its frequency over time $\dot{f}$ and by its amplitude A:

$$\dot{f} \propto M_c^{5/3} f^{11/3} + \begin{pmatrix} \text{relativistic corrections} \\ M_1, M_2, S_1, S_2 \end{pmatrix} \tag{10}$$

$$A \propto k_{\text{orbit}} M_c^{5/3} \frac{f^{2/3}}{r} \tag{11}$$

with M_c the chirp mass

$$M_c = \frac{(M_1 M_2)^{3/5}}{(M_1 + M_2)^{1/5}}, \tag{12}$$

f the orbital frequency, M_1, M_2, S_1 and S_2 the mass and spin of the two compact objects, respectively, k_{orbit} a constant accounting for the inclination of the source orbital plane and r the distance to the source. If enough binary systems are detected, one can average over orbital parameters and can use them as standard candles. (One can determine the distance from the second equation using the chirp mass from the first equation.)

Being able to determine the exact waveform of an inspiral event will also reveal additional information about the system itself (see, for example, Ref.[13]):

- harmonic content $\Rightarrow$ eccentricity of orbit
- even-odd modulation $\Rightarrow$ mass ratio of the two objects
- modulation of waveform $\Rightarrow$ spin-orbit coupling (mainly frame dragging in black-hole systems)
- higher-order corrections to waveform sweep$\Rightarrow$ individual mass and spin of constituents

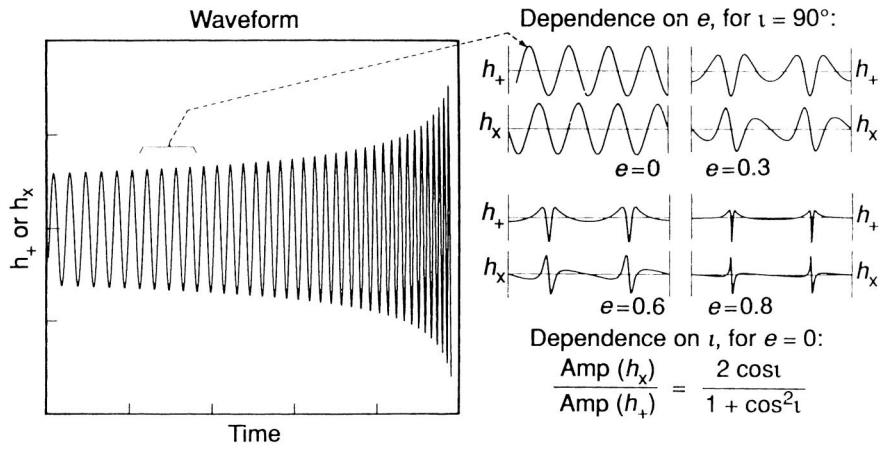

Figure 3. Chirp waveform from an inspiral event of a compact binary system. On the right hand side the dependency of the waveform on the orbital eccentricity e and the orbital inclination ι is demonstrated. The plot is taken from Ref.[14].

- end point (merger) $\Rightarrow$ large scale nuclear matter. If the nuclear state equation of a neutron star is soft the merger may happen earlier due to a hydrodynamic melting effect. On the other hand the gravitational field of the companion star may trigger the neutron start to fall into a black hole before the actual merger.

Calculating waveforms for coalescing compact binaries is straight forward, if the distance between the two objects is large, but for black hole mergers it is a formidable challenge. The coalescence of two black holes can be roughly divided into three phases:

- inspiral: The two black holes are well separated and the waveform of the emitted gravitational waveform is known,
- merger: The horizons of the two black holes merge together and the calculation of the exact waveform requires extensive simulations on a super computer, and
- linear pulsations: The two black holes have merged into a single black hole in an excited state. The excited state can be treated as a linear pulsation which decays by emitting gravitational waves.

3.2 Binary stars

Ordinary binary stars are one of the most reliably understood sources for periodic gravitational waves. Binary stars typically have orbital periods larger than an hour and, correspondingly, gravitational wave frequencies $\leq 10^{-3}$ Hz. This means that only space-based detectors will be able to detect them by integrating over long time periods (see section 4.4).

3.3 Rotating neutron stars

A rotating neutron star will emit gravitational waves if its mass distribution is non axis-symmetric along the rotation axis. A non axis-symmetric mass distribution could be due to extremely strong magnetic fields which deform the star, due to its past history which created the star in a deformed state, or due to accretion of matter from a companion star.

3.4 Neutron star instabilities

Only recently, it was recognized that gravitational radiation tends to drive the r-modes (hydrodynamic currents within the star's core) of all rotating stars unstable[15,16,17]. Gravitational radiation couples to these modes primarily through the current quadrupole, rather than the quadrupole of the mass distribution. These neutron stars can spin down to a fraction of their initial frequency within a relatively short period of time (~ 1 year).

3.5 Supernovæ

Supernovæ have all the attributes associated with a good gravitational wave source: they weigh several solar masses, they are compact and they experience large accelerations. However gravitational radiation only couples to a changing quadrupole moment and, hence, if a supernova collapse and the subsequent explosion have an axial symmetry, no gravitational waves are emitted.

There are several possible mechanisms which could overcome this deficit:

- Initial density and temperature fluctuations may trigger the collapse unevenly,
- High rotation speeds can lead to a bar instability,
- Hydrodynamic instabilities could introduce large convection streams which may effect the initial implosion

- A reminiscent neutron star may experience a strong boiling shortly after its formation.

It is unlikely that each and every supernova event will be exactly axis symmetric, but how large the asymmetries are and how often these asymmetries lead to detectable gravitational waves is very much uncertain at this time.

If a supernova is seen both in the electro-magnetic and the gravitational wave spectrum, one will also be able to compare the speed of light with the propagation speed of gravitational waves (general relativity theory predicts them to be the same).

3.6 Supermassive black holes

An other good sources of gravitational waves are supermassive black holes ($M > 10^5 M_\odot$) eating surrounding objects. However, due to their size the frequency band of interest is lower than the one for the above sources. Typical frequencies are in the mHz regime and will not be accessible by earth-based observations due to limitations posed by seismic activities and gravity gradient noise (see next chapter). However, these sources are prime candidates for space-based antennæ.

3.7 Stochastic background

Density fluctuations in the early universe can lead to a stochastic background of gravitational waves (similar to the microwave background). Measuring the spectrum of the stochastic background would connect us to the Planck area and would be a good mean to discriminate different cosmological models (inflation, cosmic strings, QCD phase transitions). However, for most models the predicted amplitude of the stochastic background is well below the sensitivity of what is technologically achievable today or in the intermediate future.

4 Laser interferometers

The idea of detecting gravitational waves using a Michelson interferometer was discovered by several groups independently[18,19,20,21], and lead to the first prototype of an interferometric detector[22,23]. The idea took a significant step forward when R. Weiss[21] performed a study which identified all the important noise sources which limit the instrumental sensitivity (see next section).

There are two complementary approaches to detect gravitational waves with laser interferometers: space-based and earth-based. A space-based an-

tenna is free from seismic excitations and can utilize long arm lengths of order 10^{10} m. It is best suited to detect gravitational waves in a frequency band between $\sim 10^{-4}$ Hz and $\sim 10^{-1}$ Hz. An earth-based antenna is limited by gravity gradient noise below a couple of Hz; in reality, seismic noise probably sets this limit even higher. Earth-based detectors have their best sensitivity in a frequency band between $\sim 10^{1}$ Hz and $\sim 10^{3}$ Hz.

4.1 Noise sources

Measuring length deviations smaller than the proton radius puts high requirements on the technology used to build these instruments. It also requires a good understanding of physical and technical noise sources which possibly limit the gravitational wave sensitivity. The design sensitivity of the Laser Interferometer gravitational wave Observatory (LIGO) Project is shown in Fig. 4. It shows that the sensitivity at low frequency, $f < 50$ Hz, is due to seismic noise, at intermediate frequencies, 50 Hz$< f < 150$ Hz, due to thermal noise and at high frequencies, $f > 150$ Hz, due to laser shot noise. The following paragraphs are listing noise sources influencing the strain measurement by directly affecting the laser light (limiting noise sources for initial earth-based interferometric detectors are shown in bold):

- **shot noise**: The fluctuations of the number of photons in the input beam causes fluctuations of the signal at the anti-symmetric port. For a power-recycled Michelson interferometer with Fabry-Perot arm cavities (see section 4.2) one obtains an equivalent shot noise limited strain sensitivity of

$$h_{\rm shot}(f) \sim \frac{\sqrt{1+(f/f_{\rm FPI})^2}}{N_{\rm bounce}} \frac{\lambda}{2\pi L} \sqrt{\frac{h\nu}{G_{\rm RC} P_{\rm in}}} \tag{13}$$

  with $f_{\rm FPI}$ the cavity pole, $N_{\rm bounce}$ the average number of effective bounces in the arms, λ and ν the laser wavelength and frequency, respectively, L the arm length, $G_{\rm RC}$ the power-recycling gain and $P_{\rm in}$ the input laser power. Fig. 5 shows the sensitivity spectrum of the phase noise interferometer at MIT[24], demonstrating that it is technically possible to achieve shot noise limited sensitivity above a couple of 100 Hz.

- light amplitude and laser frequency noise: In a perfect Michelson interferometer common-mode noise sources such as the laser amplitude and frequency noise do not propagate to the anti-symmetric port. But in

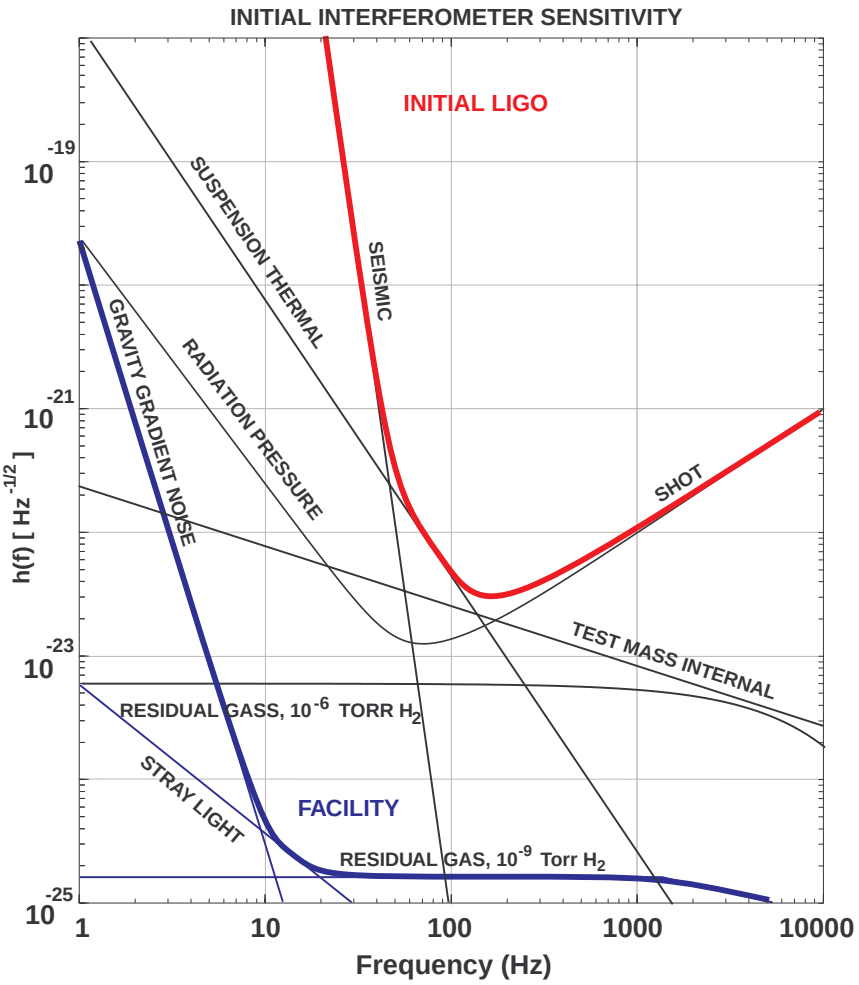

Figure 4. Design sensitivity for the Laser Interferometer Gravitational wave Observatory (LIGO). The plot shows that the initial strain sensitivity is limited by seismic, thermal and shot noise. These are technical noise sources which can be improved on in future designs. The plot also shows the gravity gradient, the scattered light and the residual gas noise which ultimately will limit the sensitivity of earth-based detectors.

reality, any small imbalance between the two Michelson arms will couple laser noise into the gravitational wave band. In a power-recycled Michelson interferometer with Fabry-Perot arm cavities, the amplitude noise mainly couples through differential deviation from resonance, whereas laser frequency noise couples through arm cavity differences in reflectivity and frequency response, and through differences in the path lengths of the Michelson. Even so these coupling coefficients are generally small, together with the required strain sensitivity, it still translates to very stringent requirements on the laser.

- oscillator phase and amplitude noise: A heterodyne detection scheme (see section 4.3) requires an oscillator to generate the rf modulation sidebands. Phase and amplitude noise of this oscillator can be coupled to the antisymmetric port through differential arm length deviations.

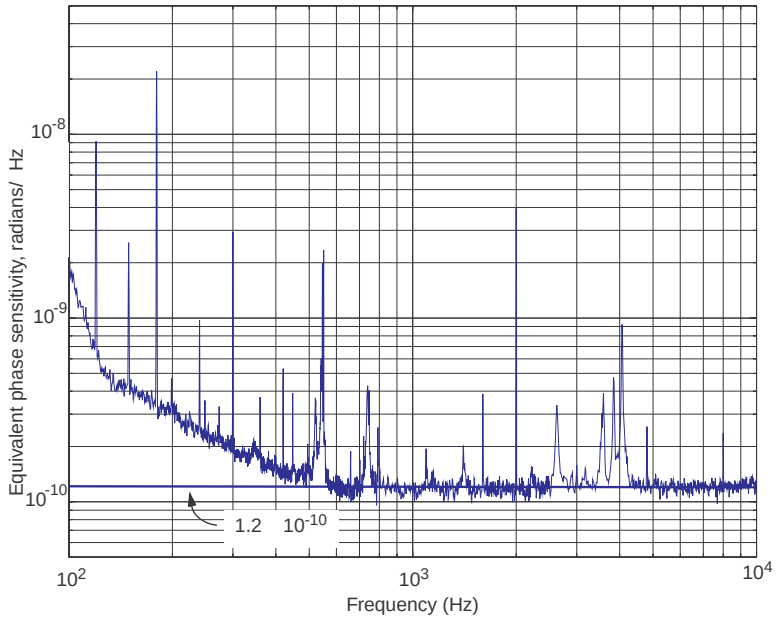

Figure 5. Spectral sensitivity of the MIT phase noise interferometer (see Ref.[24]). Above 500 Hz the spectrum is shot noise limited at a level close to the one needed for initial earth-based detectors. The additional features seen in the spectrum are due to 60 Hz powerline harmonics, wire resonances (500 Hz – 600 Hz), optical mount resonances (700 Hz – 800 Hz), calibration line (2 kHz) and resonances of the magnet standoffs ($\sim$ 4 kHz).

- scattered light: Light which scatters out of the beam path because of an imperfect optical surface and which then scatters from an outside surface back into the interferometer will produce a parasitic interference driven by the motion of the outside scattering surface. Extreme care is taken to isolate the optics of the interferometer from seismic excitations. It is important not to by-pass this isolation through parasitic interference from surfaces directly connected to the ground. Even if the motion is slow, it can be larger than a wavelength and, thus, cause an up-conversion of seismic noise to the gravitational wave band.

  Back scattering is the main reason the interferometer beams are contained in vacuum and not guided through fiber optics.

- beam jitter: Jitter of the input beam, both lateral and in angle, can couple to the anti-symmetric port through static angular misalignments of the interferometer.

- residual gas column density fluctuations: Density fluctuations in a gas induce fluctuations of the refractive index and lead to Rayleigh scattering.

Another set of noise sources cause displacement noise by introducing fluctuation forces which are moving the end points of the interferometer:

- **seismic noise**: The earth surface is in constant motion because of seismic and volcanic activities, because of ocean waves "hammering" on the shores, because of wind and because of the tidal forces of the moon. Seismic noise is most pronounced at low frequencies (0.1 Hz to 10 Hz) and falls off quickly at higher frequencies. Typical seismic noise levels are

$$x(f) \simeq 10^{-9}\ \mathrm{m}/\sqrt{\mathrm{Hz}} \qquad \text{for } 1\,\mathrm{Hz} < f \leq 10\,\mathrm{Hz} \tag{14}$$

$$x(f) \simeq \frac{10^{-7}}{f^2}\ \mathrm{m}/\sqrt{\mathrm{Hz}} \qquad \text{for } f > 10\,\mathrm{Hz} \tag{15}$$

  For initial earth-based interferometers roughly an attenuation of 9 orders of magnitude is required at frequencies around 100 Hz.

- **thermal noise in the suspension elements**: Thermally driven motions of the test masses (optical components) will limit the initial sensitivity of earth-based detectors in the intermediate frequency range around 100 Hz. The magnitude of these motions depends on $k_B T$, with k_B the Boltzmann constant and T the temperature. To investigate the effect of

thermal noise one has to look at its spectral density. There is a deeper connection between the dissipation mechanism of a system and the power spectral density of the random displacements. Low loss systems typically have high Q resonances. Most of the random motion is concentrated in a small bandwidth around these resonances. By decreasing the dissipation of a system, one can increase the Q and at the same time reduce the spectral density of the random displacements away from resonance (for a more detailed description of thermal noise see for example[25]).

A simple way to obtain a low loss system is to suspend the test masses in form of a pendulum. The restoring force of a pendulum has two components: gravity and the elasticity of the suspension wire. For all practical purposes the "gravitational spring" is lossless, and only the elastic spring constant has a dissipative fraction. As long as the wire is reasonably fine, the elastic spring constant is much smaller than the gravitational spring constant. Typically, the pendulum frequency for a suspended test mass is around $\sim$ 1 Hz. Above resonance the spectral density falls as $f^{5/2}$ (frictional damping).

The effect of thermal noise on the strain sensitivity of an interferometer is proportional to the (average) number of effective bounces of the laser beam. This is the main reason to favor a long baseline design with a low number of bounces over a shorter design with a higher number of bounces.

The sensitivity curve of the Caltech 40 m interferometer[26] is shown in Fig. 6. It clearly demonstrates the importance of thermal noise.

- **thermal noise driving mirror normal modes**: The equipartition theorem states that every eigenmode of a system is excited by thermal noise to a mean energy of $k_B T/2$. This is also true for the "drum" modes of the test masses. Typically, the frequencies of these eigenmodes is in the kHz regime.

- radiation pressure imbalance: The number of photons hitting either end test mass will fluctuate due to the photon count statistics. The recoil of these photons will then introduce a small force which pushes on the test masses. For a power-recycled Michelson interferometer with Fabry-Perot arm cavities one obtains a radiation pressure equivalent strain sensitivity of

$$h_{\gamma P}(f) \simeq \frac{2}{\pi^2} N_{\mathrm{bounce}} \frac{\sqrt{G_{\mathrm{RC}} P_{\mathrm{in}} h\nu}}{LMcf^2} \tag{16}$$

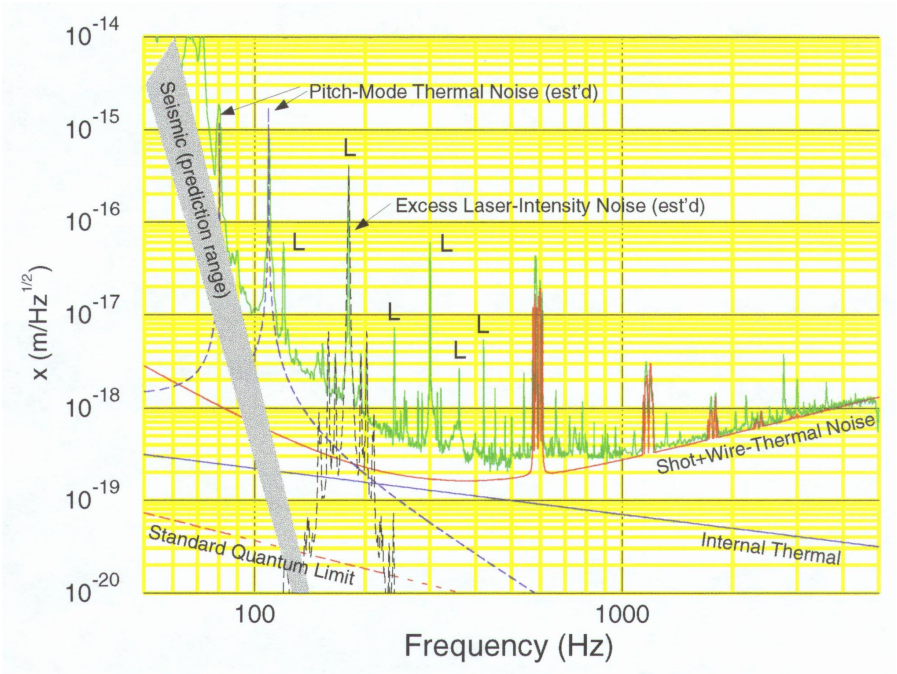

Figure 6. Spectral sensitivity of the Caltech 40 m interferometer (see Ref.[26]). It shows a displacement sensitivity comparable to the one of initial earth-based interferometers. The seismic noise prediction is an empirical one based on measurements of the ground noise and the transfer function of ground motion to interferometer displacement. The thermal noise prediction is a theoretical one based on measured frequencies and Q's for various modes and the assumption that the loss function is a constant for each mode. The shot noise curve is calculated theoretically and has been confirmed experimentally to within $\sim 20\%$. The broad peaks near 600, 1200 and 1800 Hz are sets of narrow violin-mode resonances of the test mass suspension wires excited by thermal noise which blend together in this relatively low resolution (approximately 1 Hz bandwidth) spectrum. The remaining peaks are largely instrumental artifacts. The most numerous are powerline frequency harmonics caused by electrical interference (marked "L") in the electronics used for this measurement. The peaks at 80 and 109 Hz are pendulum pitch-mode resonances.

with M the mass of the optical components. If one combines Eq. (13) and Eq. (16), one can see that without increasing the test mass there is a natural limit for a given frequency on how much one can increase the laser power to reduce the shot noise, before the radiation pressure noise becomes a problem.

- "radiometer" force: Photons absorbed in the mirror coating can transfer their energy to molecules which are bouncing off the mirror surface. The increased recoil of these molecules will apply an additional force to a test mass.

- gravity gradients: Any mass placed nearby an optical component will apply a force through gravity. Moving masses such as seismic waves compressing the earth and density fluctuations in the air are the main concerns, since they give rise to gravity gradients. For earth-based detectors this will set the ultimate limit in sensitivity at very low frequencies.

- electric field fluctuations: Varying external electric fields together with a (induced) surface charge can also affect a test mass.

- magnetic field fluctuations: Presently, most suspended test masses incorporate actuators for the active control system which consist of permanent magnets glued to the back of the test mass and a coil driver mounted to the suspension cage. External magnetic fields can then apply a force to a test mass, either, through an imbalance in the magnets or through field gradients.

- cosmic ray muons: Cosmic ray muons can be produced at high altitude when a high energy proton enters the earth atmosphere. Because the cross-section of muons is small they can reach the ground and in some rare cases stop in a test mass. The recoil of the muon then looks like a "random" force.

4.2 Interferometer configurations

Most modern designs implement improved versions of a simple Michelson interferometer (see Fig. 7). A simple Michelson interferometer has an antenna response function $A(\Omega)$ which is proportional to (see the appendix on how to derive an interferometer response function):

$$A(\Omega) \propto \operatorname{sinc}\left(\frac{\Omega L}{c}\right) \qquad \text{Michelson} \tag{17}$$

with $\operatorname{sinc} x = \sin x/x$, Ω the angular frequency of the gravitational wave and L the length of each arm. Putting numbers into Eq. (17) shows that for frequency between 10 Hz and 1 kHz, the optimal antenna length is of order 10^5 m to 10^7 m. This is much larger than would be feasible for an earth-based detector. However, there is no reason that the arm of a Michelson

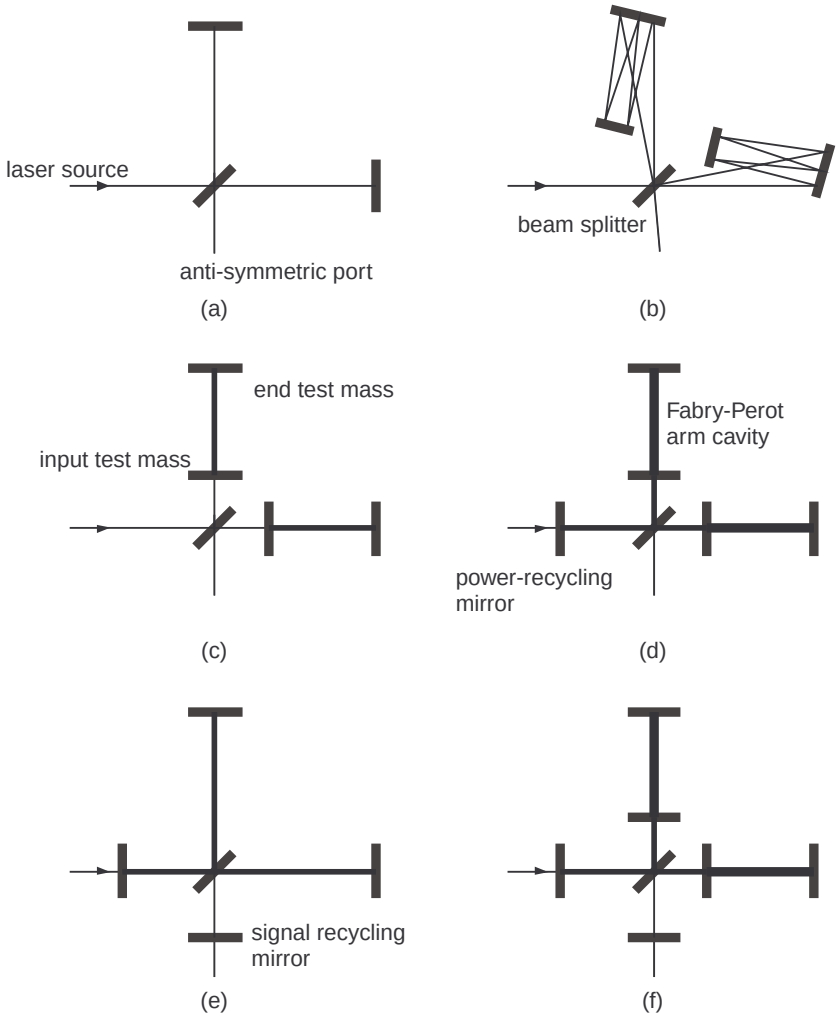

Figure 7. Possible interferometer configurations for gravitational wave detectors: simple Michelson interferometer (a), Michelson with delay lines (b), Michelson with Fabry-Perot arm cavities (c), power-recycled Michelson with Fabry-Perot arm cavities (d), dual recycled Michelson (e) and dual recycled Michelson with Fabry-Perot arm cavities (f). There are many more configurations; some of them are mentioned in the text.

interferometer cannot be folded[27]. Indeed, this configuration is known as a delay line and its antenna function is proportional to:

$$A(\Omega) \propto \mathrm{sinc}\left(N\frac{\Omega L}{c}\right) \qquad \text{delay line} \tag{18}$$

where N describes the number of folds (number of bounces). In practice, this configuration has a couple of disadvantages:

- If the number of folds is large, the mirror which is used to bounce the laser beams forth and back, has to be large as well. This is compounded by the fact that for long baseline interferometers the diffraction limited beam diameter is of order 10 mm to 100 mm.
- Light scattered by an imperfect mirror away from the nominal angle of reflection can interfere with the light from neighboring light passes and ruin the instrumental sensitivity.

A similar effect to folding the light pass N times can be achieved by inserting a Fabry-Perot cavity into each arm of the Michelson[28,29,30]. A Fabry-Perot cavity consists of a partially transmitting input mirror and a high reflective rear mirror. If the length of the Fabry-Perot is adjusted to a multiple of the laser wavelength the cavity becomes resonant. The light power inside the cavity builds up and simulates the effect of sending the light forth and back multiple times. However, in this case the number of bounces is not a fixed quantity, but rather an averaged effective value. Both the problem of the mirror size and the scattering is now much reduced, since the multiple light paths are now lying on top of each other. But, a Fabry-Perot cavity has to be hold on resonance during operations which requires an active control system. The antenna function of a Michelson interferometer with Fabry-Perot arm cavities can be written as[31,32]:

$$A(\Omega) \propto \mathrm{sinc}\left(\frac{\Omega L}{c}\right)\mathrm{FPI}(\frac{\Omega L}{\pi c}) \qquad \begin{array}{l}\text{Michelson with}\\ \text{Fabry-Perot arm cavities}\end{array} \tag{19}$$

The Fabry-Perot response function (power build-up inside the cavity) depends on the input and rear mirror amplitude reflectivity coefficients, r_1 and r_2, respectively, and the input mirror amplitude transmission coefficient t_1 (see for example Ref.[33]).

$$\mathrm{FPI}(x) = \left|\frac{t_1}{1 - r_1 r_2 e^{ix}}\right|^2 \tag{20}$$

If the mirrors have low optical losses and if the rear mirror is a high reflector, most of the power incident to a Fabry-Perot arm cavity will be reflected back to the beam splitter. Ideally, the anti-symmetric port of the Michelson interferometer is set on a dark fringe to minimize shot noise. Then a differential length change induced by a gravitational wave will leave through the anti-symmetric port with the highest possible signal-to-noise ratio. This in turn means that most of the injected light will leave the interferometer through the symmetric port and be lost. But, by placing an other partially transmitting mirror at input one can form yet another cavity—the power recycling cavity—and recycle most of the otherwise lost light[34]. The interferometer response is then enhanced by the power recycling gain (additional power build-up in the power recycling cavity).

$$A(\Omega) \propto \operatorname{sinc}\left(\frac{\Omega L}{c}\right) \mathrm{FPI}(\frac{\Omega L}{\pi c})\, G_{\mathrm{RC}} \qquad \begin{array}{l}\text{Power-recycled}\\ \text{Michelson with}\\ \text{Fabry-Perot arm cavities}\end{array} \tag{21}$$

By adding a partially transmitting mirror to the anti-symmetric output port the gravitational wave signal can be made resonant[35,36]. This makes it possible to shape the interferometer response, so that its sensitivity is improved in a narrow frequency band around the signal resonance. In general, this means that the sensitivity outside the resonant frequency band will be worse. This is not a problem at lower frequencies where the interferometer is usually limited by seismic noise. If both power and signal recycling are implemented the configuration is called dual recycled.

The above configurations are the most common ones currently implemented or designed, but there other possible layouts such as Sagnacs[37], configurations with an output mode cleaner, resonant recycling where the beam splitter is turned by 90° to directly couple the two arm cavities[34], and many more.

4.3 Detection schemes

Most interferometer configurations require an active control system to keep cavities locked to a resonance, or to keep the anti-symmetric port on a dark fringe, respectively. To be able to implement a feedback system one first needs an error signal which measures the microscopic longitudinal deviations. Neither of the above conditions would allow for simply monitoring the power levels, since moving away from resonance or away from a dark fringe will decrease or increase the power levels, respectively, without indicating the direction of the deviation. One could solve this problem by putting the "working

point" of the feedback control system off resonance and towards mid fringe. But, this technique makes both power and signal recycling impossible.

All currently built and planned interferometers therefore implement a heterodyne detection scheme[21]. Historically, the first heterodyne detection schemes implemented a longitudinal dither of the cavities. This in turn modulates the power in the cavity and, if off-resonance, yields an error signal at the dither frequency. However, a laser source typically becomes shot noise limited at radio frequencies (rf) only, well above dither frequencies which are achievable in the lab.

A better scheme—the Pound-Drever-Hall reflection locking technique[28,29,30]—imposes phase modulate rf sidebands on the laser light itself. An off-resonance cavity then acts as an FM-to-AM converter yielding error signals at the rf frequency. The gravitational wave readout port usually implements a suppressed carrier scheme[39]. A differential length deviation will produce a signal at the carrier frequency leaking out the anti-symmetric port, which then beats against constant rf sidebands.

4.4 LISA: A space-based interferometer

The LISA (Laser Interferometer Space Antenna) Project[a,40] is a planned space mission, adopted by ESA and NASA, to deploy 3 satellites in solar orbit forming a large equilateral triangle with a base length of 5×10^6 km. The center of the triangle formation will be in the ecliptic plane 1 AU from the sun and 20 degrees behind the earth. The main objective of the LISA mission is to observe low frequency (10^{-4} Hz to 10^{-1} Hz) gravitational waves from galactic and extra-galactic binary systems, including gravitational waves generated in the vicinity of the very massive black holes found in the centers of many galaxies. The three LISA spacecrafts flying in formation will act as a giant Michelson interferometer, measuring the distortion of space caused by passing gravitational waves. Each spacecraft will contain two free-floating "proof masses". Lasers in each spacecraft will be used to measure changes in the optical path lengths with a precision of 20 pm. If approved, the project will start in the year 2005 with a planned launch in 2008.

A sensitivity plot is shown in Fig. 8. The primary goal of the LISA mission is to detect and study in detail gravitational wave signals from sources involving massive black holes. LISA will certainly observe distinguishable signals from thousands of binary systems containing compact stars, and be able to determine the number and distribution of such binaries in our galaxy.

[a] home pages: http://www.lisa.uni-hannover.de
http://lisa.jpl.nasa.gov

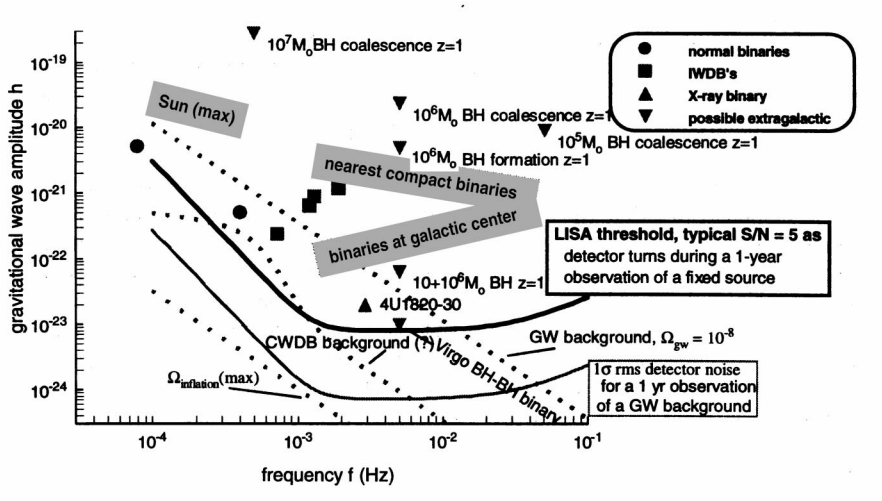

Figure 8. Sensitivity curve of the Laser Interferometer Space Antenna (LISA). Most of the LISA sources will be approximately monochromatic. The bold curve is the 1-year threshold curve, the amplitude that could be detected with confidence by a single (2-arm) LISA interferometer; it is drawn at the signal-to-noise (SNR) ratio of 5 for a fixed source that is observed by LISA for a full year.
The gravitational wave amplitude h is shown for different types of periodic and quasiperiodic sources. The expected signals from some known binaries are indicated. The nearest neutron star and white dwarf binaries at any frequency should lie in the band labeled "nearest compact binaries"; the band below that shows the amplitude expected from "typical" white dwarf binaries near the galactic center. Interacting white dwarf binaries (IWDB) are systems where a low-mass degenerate helium star fills its Roche lobe and transfers mass onto a more massive white dwarf. The shortest period stellar mass black hole binary in the Virgo cluster might be in the position shown.
The strongest sources in the diagram are binaries of massive black holes at cosmological distances, observed as they coalesce due to the orbital emission of gravitational waves. They have been placed in the diagram rather arbitrarily at their coalescence frequency and at an amplitude that correctly shows their SNR in relation to the heavy threshold curve, for a distance $z = 1$.
The 1-σ gravitational wave noise produced by a possible cosmological background left from the big bang is shown here at an energy density per decade of frequency today that is 10^{-8} of the total needed to close the universe. An upper limit to that generated by inflation is also shown. There may be more galactic close white dwarf binaries (CWDB) than LISA can resolve; a possible but uncertain effective noise level is shown. For comparison with these backgrounds, we have drawn the LISA rms noise level (faint lower curve).
The band labeled "SUN (max)" is where solar $g-$modes might produce strong near zone (Newtonian) gravitational perturbations observable by LISA. The plot is taken from Ref.[40].

Table 3. List of earth-based laser interferometers projects currently under construction worldwide.

project	**length**	**site**	**configuration**
GEO[b]	600 m	Hannover, Germany	dual recycled
LIGO[c]	4000 m 2000 m 4000 m	Hanford (WA), USA Livingston (LA), USA	power-rec. Fabry-Perot
TAMA[d]	300 m	Tokyo, Japan	dual recycled
VIRGO[e]	3000 m	Pisa, Italy	power-rec. Fabry-Perot

4.5 The LIGO Project

The Laser Interferometer Gravitational wave Observatory[14] is one of the new projects to build the next generation of gravitational wave detectors. A list of all projects currently under construction is shown in Table 3.

The essential attributes of the LIGO Project are:

- collaboration between the California Institute of Technology and the Massachusetts Institute of Technology,
- two widely separated sites under common management to make coincidence measurements,
- a vacuum system to accommodate interferometers with 4 km arm length,
- the capability to operate several interferometers at each site simultaneously,
- the ability to accommodate interferometers of two different arm lengths, 4 km and 2 km (at one site),
- a clear aperture for the laser beam of ~ 1 m,
- An ultimate vacuum of 10^{-9} torr hydrogen and 10^{-10} torr of other gases,

[b]home page: http://www.geo600.uni-hannover.de
[c]home page: http://www.ligo.caltech.edu
[d]home page: http://tamago.mtk.nao.ac.jp
[e]home page: http://www.pg.infn.it/virgo

- a physical environment monitor for detecting vetos caused by external disturbances and
- a facility lifetime of at least 20 years to do astrophysical research with gravitational waves.

All earth-based interferometric gravitational wave detectors share a similar design philosophy. The design of these detectors is driven by the goal to minimize the effect of noise on the instrumental sensitivity (see section 4.1). All designs use in-vacuum suspended optics build on top of a seismic isolation system for their main interferometer mirrors. Similarly, all designs use a highly stabilized laser source in conjunction with a mode cleaner to deliver a high quality laser beam to the interferometer. They all incorporate an optical configuration which requires an active control system for microscopically adjusting cavity and Michelson lengths, in order to counteract drifts and fluctuations introduced by seismic activities.

A brief description of the main detector components of LIGO is given below:

- laser source: The light source is a solid state diode-pumped Nd:YAG laser, consisting of a nonplaner master oscillator and a power amplifier. The nominal output power is 10 W single mode at a wavelength of 1064 nm. The laser is locked to a reference cavity to stabilize its frequency and is spatially filtered by a pre-mode cleaner. Pockels cells are used to impose phase modulated sidebands on the laser light before it is launched into the mode cleaner.
- input mode cleaner: The mode cleaner is a triangular cavity with the purpose to further filter and stabilize the laser beam.
- seismic isolation system: The seismic isolation system is a a vibration isolation stack, constructed of heavy steel plates separated by coil springs. This forms a coupled pendulum system, giving a damping factor proportional to f^{-2} above resonance for each stage.
- suspensions: All major optical components are suspended to form a pendulum using one single loop of 0.012 in. diameter steel music (piano) wire. The pendulum frequencies are typically below 1 Hz and the mass of a large mirrors is $\sim$ 10 kg. Four permanent magnets are glued to the back to control longitudinal and angular orientation of the test mass, and two magnets are glued to the side to control sideways motions. Corresponding coil drivers are mounted to the suspension cage, making it

possible to adjust the force applied to the mirror by adjusting the electric current through the coil.

- optics: A diffraction limited laser beam which spot is of similar sizes at the input and end test mass must have a waist size of order ~ 30 mm – ~ 40 mm. This requires rather large optics. In case of LIGO the masses are circular cylinders fabricated from pieces of high-purity fused silica with bulk absorption of less than 5 ppm/cm. They are 25 cm in diameter and 10 cm thick. To minimize scatter and absorption losses it is crucial to have a very good surface figure and a very low loss (≤ 1 pmm), very high uniformity coating. Surface figures of $\lambda/1000$ rms over the the central 8 cm diameter have been achieved (after coating).

- sensing and control system: Multiple InGaAs photodetectors are used at anti-symmetric port and for the auxiliary extraction ports to sense 4 longitudinal degrees-of-freedom and 14 angular degrees-of-freedom. The signal is first down-converted into the baseband and then sampled by a digitizer. Most servo functions are implemented in software, and the signals are send to the suspension controllers through fiber optics.

The planned completion dates for the LIGO Hanford 2 km system are are shown below:

beam tube	completed, currently baked
vacuum system	installed and baked
seismic isolation	installation started
laser source	installation started
mode cleaner	end of 1998
vertex Michelson	spring 1999
full interferometer	2000
engineering tests	2001
first data run	2002 and 2003

5 Conclusions

The direct observation of gravitational waves will allow to test general relativity theory by giving direct evidence of a time-dependent metric far away from the source and by independently probing strong field gravity[41,11]. It will also provide a new and different view of astrophysical processes hidden from electro-magnetic astronomy, such as the inner dynamics of supernova and neutron star cores, or such as the coalescence phase of neutron star and black hole mergers. Eventually, it may be possible to discriminate cosmological models by observing or setting a limit to the stochastic background.

The new generation of gravitational wave detectors, currently under construction, has the potential to open this new field of physics and may result in new and unexpected discoveries.

There are also certain risks associated with "stepping into a unknown territory": Are there enough strong astrophysical sources for gravitational waves? And, will the technology work at the required level? However, a direct detection of gravitational waves will almost certainly bring invaluable advance of our experimental knowledge of the universe.

Acknowledgments

I would like to thank my colleges of the LIGO collaboration for many stimulating discussions and for providing the opportunity of participating on a very interesting and challenging experiment. The LIGO Project is supported by the National Science Foundation grant PHY–9210038.

Appendix: Interferometer response function

This appendix demonstrates the techniques to calculate the antenna response function of an interferometric gravitational wave detector. We use a power recycled Michelson interferometer with Fabry-Perot arm cavities as an example.

The coordinate system is chosen to be aligned with the two arms of the interferometer, where the origin is positioned at the beam splitter and the z-axis points vertically upwards. Spherical coordinates are defined by

$$r = \begin{pmatrix} rsin\theta cos\phi \\ r\sin\theta\sin\phi \\ r\cos\theta \end{pmatrix} \qquad \text{with} \begin{cases} 0 \le \theta < 2\pi \\ 0 \le \phi < \pi \end{cases} \tag{22}$$

We then define the rotation operator $O(\theta, \phi)$ which rotates the z-axis in the direction of r:

$$O(\theta, \phi) = O(\phi)O(\theta) \tag{23}$$

$$\text{where } O(\phi) = \begin{pmatrix} \cos\phi & -\sin\phi & 0 \\ \sin\phi & \cos\phi & 0 \\ 0 & 0 & 1 \end{pmatrix} \text{ and } O(\theta) = \begin{pmatrix} \cos\theta & 0 & \sin\theta \\ 0 & 1 & 0 \\ -\sin\theta & 0 & \cos\theta \end{pmatrix} \tag{24}$$

We write the phase of the light which is acquired in one round-trip in one of the interferometer arms as

$$\Phi_{rt}(t_0) = \int_{t_0}^{t_0+t(2L)} dt\, \omega \tag{25}$$

where L is the length of the arm, ω is the angular frequency of the light and t_0 the time the photon leaves the origin. We now change the integration over time into one over length by using

$$d\tau^2 = dx^\mu g_{\mu\nu} dx^\nu 0 \quad \text{with} \quad g_{\mu\nu} = \eta_{\mu\nu} + h_{\mu\nu} \tag{26}$$

where $\eta_{\mu\nu}$ is the Minkovski metric and $h_{\mu\nu}$ is the space-time ripple due to the gravitational wave. For a gravitational wave traveling along the z-axis, $h_{\mu\nu}$ becomes in the transverse-traceless gauge[8]

$$h_{\mu\nu} = \cos(\Omega t - kz) \begin{pmatrix} 0 & 0 & 0 & 0 \\ 0 & & & \\ 0 & & \hat{H}_{ik} & \\ 0 & & & \end{pmatrix} \quad \text{with } \hat{H}_{ik} = \begin{pmatrix} h_+ & h_\times & 0 \\ -h_\times & h_+ & 0 \\ 0 & 0 & 0 \end{pmatrix} \tag{27}$$

where Ω is the angular frequency of the gravitational wave, k is its wave vector, h_+ and $h_\times$ are the wave amplitudes for the"+" and the "×" polarization, respectively.

For arbitrary directions one has to rotate both z and $\hat{H}_{ik}$ in the direction of the wave vector k.

$$kz \rightarrow k(k_x x + k_y y + k_z z) \quad \text{with } \begin{cases} k_x = \sin\theta\cos\phi \\ k_y = \sin\theta\sin\phi \\ k_z = \cos\theta \end{cases} \tag{28}$$

$$\hat{H}_{ik} \rightarrow H_{ik} = O(\theta,\phi)\hat{H}_{ik}O(\theta,\phi)^{-1} \equiv \begin{pmatrix} h_{xx} & h_{xy} & h_{xz} \\ h_{yx} & h_{yy} & h_{yz} \\ h_{zx} & h_{zy} & h_{zz} \end{pmatrix} \tag{29}$$

For an integration along the x-axis or the y-axis h_{xx} and h_{yy} are the only relevant matrix elements, respectively.

$$h_{xx} = -\cos\theta\sin 2\phi\, h_\times + (\cos^2\theta\cos^2\phi - \sin^2\phi)\, h_+ \tag{30}$$

$$h_{yy} = \cos\theta\sin 2\phi\, h_\times + (\cos^2\theta\sin^2\phi - \cos^2\phi)\, h_+ \tag{31}$$

Fig. 9 shows the angular dependence of $\mid h_{xx} - h_{yy} \mid$ for both polarization and the average. Using Eq. (25) we rewrite Eq. (26) as

$$\Phi^x_{rt}(t_0) = \frac{\Omega}{c}\int_0^L dx\,\{\,\sqrt{1 + h_{xx}\cos(\Omega t_0 + k(1-k_x)x)} + \sqrt{1 + h_{xx}\cos(\Omega t_0 + k(2L - (1+k_x))x)}\Big\} \tag{32}$$

Similarly, $\Phi^y_{rt}(t_0)$ can be obtained by integrating along the y-axis. Since $h_{xx} \ll 1$ we can expand the square root of Eq. (32) in a Taylor series. Performing the integration, keeping only time-dependent terms, time-shift from departure to arrival, and changing to a complex notation where the absolute value denotes the amplitude and the argument denotes the phase shift, one gets:

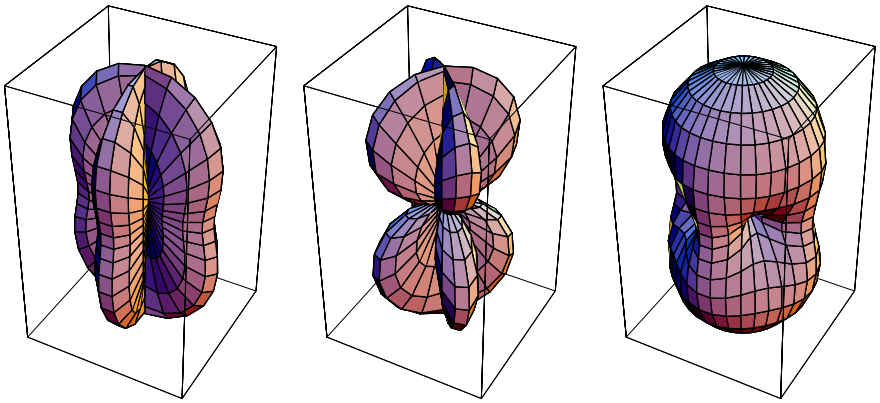

Figure 9. Antenna response function for an interferometric gravitational wave detector. The interferometer is placed at the center of the surrounding box with Michelson arms oriented along the horizontal axes. The distance from a point of the plot surface to the center of the box is a measure for the gravitational wave sensitivity in this direction. The plot to the left is for + polarization, the middle one for × polarization and the right one for unpolarized waves.

$$\Delta\Phi^x_{rt} = \frac{h_{xx}L\omega}{c} e^{i\Phi_\Omega} \frac{\sin\Phi_\Omega + ik_x\cos\Phi_\Omega - ik_x e^{ik_x\Phi_\Omega}}{\Phi_\Omega(1-k_x^2)} \tag{33}$$

$$\simeq \frac{h_{xx}L\omega}{c} \mathrm{sinc}\,\Phi_\Omega \cos(\frac{k_x\Phi_\Omega}{\sqrt{12}}) e^{i(1+k_x/2)\Phi_\Omega} \tag{34}$$

where $\Phi_\Omega = L\Omega/c$ and $\mathrm{sinc}\,x$ denotes $\sin x/x$. The approximation yields the exact solution for a gravitational wave traveling along the z-axis. From Eq. (34) one sees that the signal delay for photons arriving at the origin is $1 + k_x/2$ times half the round-trip time. The finite time a photon spends in a Michelson arm also leads to a small correction of the signal amplitude which would otherwise be determined by $h_{xx}L$ only. Fig. 10 shows the amplitude correction and time delay of the round trip phase of a gravitational wave as function of k_x relative to one of normal incident and strength h_{xx}. These effects are generally small and in most cases negligible.

To calculate the response of a cavity to a gravitational wave of a certain frequency Ω we write the electric field as a three-component vector denoting the carrier field, the upper audio sideband with frequency $+\Omega$ and the lower audio sideband with frequency $-\Omega$. The round-trip operator $X(\Omega)$ can be

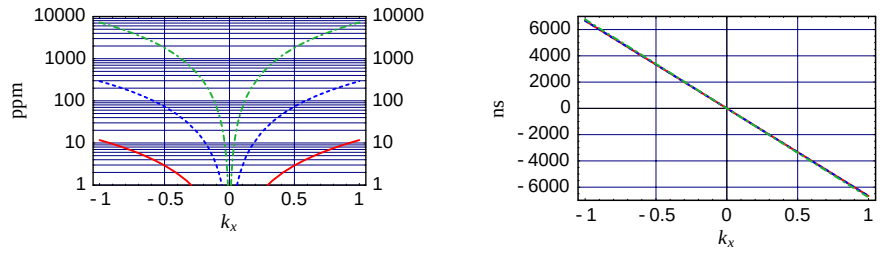

Figure 10. Amplitude correction and time delay for non normal incidence. For details see text.

expressed as[42]

$$X(\Omega) = \begin{pmatrix} 1 & 0 & 0 \\ -\frac{i}{2}\Delta\Phi_{rt}\, e^{-2i\Omega L/c} & 0 \\ -\frac{i}{2}\Delta\Phi^*_{rt} & 0 & e^{2i\Omega L/c} \end{pmatrix} \tag{35}$$

where we neglected the factor $e^{-2i\omega L/c+2i\eta}$ which is unity when the cavity is on resonance (with η the Gouy phase shift). The reflected field operator for a cavity then becomes

$$X_{\rm refl}(\Omega) = \Big(r_1 - (r_1^2 + t_1^2)\sqrt{1-\delta}\; X(\Omega)\Big)\Big(1 - r_1\sqrt{1-\delta}\, X(\Omega)\Big)^{-1} \tag{36}$$

where r_1 and t_1 are the amplitude reflectivity and transmission coefficients of the input mirror and δ is the total round-trip loss (including the reflectivity of the rear mirror). Using a carrier only in the input field $E_{\rm in}$, the reflected audio sidebands become

$$E^{+\Omega}_{\rm refl} = \frac{i}{2} G_{\rm refl}(\Omega)\, \Delta\Phi_{rt}\, e^{i\Omega t} E_{\rm in} \quad \text{and} \quad E^{-\Omega}_{\rm refl} = \frac{i}{2} G^*_{\rm refl}(\Omega)\, \Delta\Phi^*_{rt}\, e^{-i\Omega t} E_{\rm in} \tag{37}$$

$$G_{\rm refl}(\Omega) = \frac{\sqrt{1-\delta}\, t_1^2}{(1-\sqrt{1-\delta}\, r_1))(1-\sqrt{1-\delta}\, r_1 e^{-2i\Omega L/c})} \tag{38}$$

$$\simeq \frac{\sqrt{1-\delta}\, t_1^2}{(1-\sqrt{1-\delta}\, r_1)^2}\; \frac{e^{i\Omega L/c}}{1 + i\frac{\Omega}{\omega_{\rm cav}}} \qquad \text{for } \Omega \ll \frac{c}{2L} \tag{39}$$

and with the cavity pole at $\omega_{\rm cav} = \dfrac{1 - r_1\sqrt{1-\delta}}{\sqrt{r_1\sqrt{1-\delta}}}$ (40)

The audio sideband signal can be simplified to

$$E^{+\Omega}_{\rm refl} + E^{-\Omega}_{\rm refl} = \mid G(\Omega)\,\Delta\Phi_{rt} \mid \cos(\Omega t + \arg(G(\Omega)\,\Delta\Phi_{rt}))E_{\rm in} \quad (41)$$

$$\equiv \mid g \mid \cos(\Omega t + \arg g) \quad (42)$$

The signal at the anti-symmetric port is then given by

$$E_{\rm anti} = i\,t_{bs}r_{bs}\left\{\sqrt{1-\delta_x}\,g_x\cos(\Omega t + \arg g_x) - \sqrt{1-\delta_y}\,g_y\cos(\Omega t + \arg g_y)\right\}E_{\rm RC} \quad (43)$$

where r_{bs} and t_{bs} are the amplitude reflectivity and transmission coefficients for the beam splitter, respectively, δ_x and δ_y are the losses in the (short) inside Michelson arms for the incident carrier light and the reflected gravitational wave signal, g_x and g_y denote the signals from the in-line and the off-line arm cavities, respectively, and $E_{\rm RC}$ is the carrier field incident on the beam splitter. We now write the rf sideband signal at the anti-symmetric port as

$$E^{\rm sb}_{\rm dark} = 2i|E_{\rm sb}|\sin\omega_m t \quad (44)$$

where $|E_{\rm sb}|$ is the field strength of either rf sideband and ω_m is the angular modulation frequency. Down-converting the signal yields

$$V_{\rm dark} = R\sin\omega_m t\,\epsilon_{\rm PD}|E^{\rm sb}_{\rm dark} + E_{\rm dark}|\,d^2 \quad (45)$$

$$\stackrel{\rm dc}{=} \sqrt{32}R\,\epsilon_{\rm PD}\sqrt{P_{\rm RC}P_{\rm sb}}\,t_{bs}r_{bs}\left\{\sqrt{1-\delta_x}\,G_x(\Omega)\,\Delta\Phi^x_{rt} - \sqrt{1-\delta_y}\,G_y(\Omega)\,\Delta\Phi^y_{rt}\right\} \quad (46)$$

On the last line we returned to the complex notation where the absolute value denotes the signal amplitude and where the argument denotes the signal phase shift. R is the transimpedance gain of the mixer, filter, amplifier circuit chain, $\epsilon_{\rm PD}$ is the efficiency of the photodetector, $P_{\rm RC}$ and $P_{\rm sb}$ are the carrier power on the beam splitter and the total sideband power at the anti-symmetric port, respectively.

References

1. A. Einstein, Preuss. Akad. Wiss. Berlin, Sitzungsberichte der physikalisch-mathematischen Klasse , 688 (1916).
2. A. Einstein, Preuss. Akad. Wiss. Berlin, Sitzungsberichte der physikalisch-mathematischen Klasse , 154 (1918).
3. R.A. Hulse and J.H. Taylor, Astrophys. J. **191**, L59–L61 (1974).
4. R.A. Hulse and J.H. Taylor, Astrophys. J. **195**, L51–L53 (1975).
5. R.A. Hulse and J.H. Taylor, Astrophys. J. **201**, L55–L59 (1975).
6. J.H Taylor, L.A. Fowler and P.M. McCulloch, Nature **277**, 437 (1979).
7. K.S. Thorne, *Gravitational Radiation*, in *300 Years of Gravitation*, eds. S.W. Hawking and W. Israel (Cambridge U. Press, Cambridge, UK, 1987); and references therein.
8. C.W. Misner, K.S. Thorne and J.A. Wheeler, *Gravitation* (W.H. Freeman and Copmpany, New York, 1973).
9. K.S. Thorne, in *Proceedings of the XXII SLAC Summer Institute on Particle Physics*, eds. J. Chan and L. DePorcel (SLAC Report 484, Standford, 1996), 41.
10. J.H Taylor, *Noble lecture: Binary Pulsars and Relativistic Gravity*, Rev. Mod. Phys. , 711–719 (1994).
11. T. Damour and G. Esposito-Farèse, Phys. Rev. D **58**, 042001 (1998).
12. B.F. Shutz, Nature **323**, 310 (1986).
13. C. Cutler and E.E. Flanagan, Phys.Rev. **D49**, 2658-2697 (1994).
14. A. Abramovici, W.E. Althouse, R.W.P. Drever, Y. Gürsel, S. Kawamura, F.J. Raab, D. Shoemaker, L. Sievers, R.E. Spero, K.S. Thorne, R.E. Vogt, R. Weiss, S.E. Whitcomb and M.E. Zucker, Science **256**, 325–333 (1992).
15. N. Anderson, gr-gc/9706075, to be published in Astrophys. J.
16. L. Lindblom, B.J. Owen and S.M. Morsink, Phys. Rev. Lett. **80**, 4843–4846 (1998).
17. N. Anderson, K.D. Kokkotas and B.F. Schutz, astro-ph/9805225.
18. F.A.E. Pirani, Acta Physica Polonica **15**, 389 (1956).
19. M.E. Gertsenshtein and V.I. Pustovoit, Soviet Phyics – JETP **14**, 433 (1962).
20. J. Weber, unpublished.
21. R. Weiss, Quarterly Progress Report of the Research Laboratory of Electronics of the Massachusetts Institute of Technology **105**, 54 (1972).
22. G.E. Moss, L.R. Miller and R.L. Forward, Appl. Opt. **10**, 2495 (1971).
23. R.L. Forward, Phys. Rev. D **17**, 379 (1978).
24. P. Fritschel, G. Gonzàlez, B. Lantz, P. Saha, M.E. Zucker, Phys. Rev. Lett. **80**, 3181–3184 (1998).

25. P.R. Saulson, *Fundamentals of Interferometric Gravitational Wave Detectors* (World Scientific, Singapore, 1994).
26. A. Abramovici, W. Althouse, J. Camp, J.A. Giaime, A. Gillespie, S. Kawamura, A. Kuhnert, T. Lyons, F.J. Raab, R.L. Savage Jr., D. Shoemaker, L. Sievers, R. Spero, R. Vogt, R. Weiss, S. Whitcomb and M. Zucker, Phys. Lett. A **218**, 157–163 (1996).
27. D. Herriot, H. Kogelnik and R. Kompfner, Appl. Opt. **3**, 523 (1964).
28. R.W.P. Drever, G.M. Ford, J. Hough, I. Kerr, A.J. Munley, J.R. Pugh, N.A. Robertson and H. Ward, *Proceedings of the Ninth International Conference on General Relativity and Gravitation*, ed. E. Schmutzer (VEB Deutscher Verlag der Wissenschaft, Berlin, Germany, 1980).
29. A. Schenzle, R. DeVoe and G. Brewer, Phys. Rev. A **25**, 2606–2621 (1982).
30. R.W.P. Drever, J.L Hall, F.V. Kowalski, J. Hough, G.M. Ford, A.J. Munley and H. Ward, Appl. Phys. B **31**, 97–105 (1983).
31. Y. Gürsel, P. Linsay, P. Saulson, P. Spero, R. Weiss and S. Whitcomb, unpublished Caltech/MIT manuscript (1983).
32. B.J. Meers, Phys. Lett. A **142**, 465–470 (1989).
33. A.E. Siegman, *Lasers* (University Science Books, Mill Valley, CA 94941, USA, 1986).
34. R.W.P. Drever, in *Gravitational Radiation*, eds. N. Deruelle and T. Piran (North-Holland, Amsterdam, Netherlands, 1983), 321.
35. B.J. Meers, Phys. Rev. D **38**, 2317–2326 (1988).
36. J. Mizuno. K.A. Strain, P.G. Nelson, J.M. Chen, R. Shilling, A. Rüdiger, W. Winkler and K. Danzmann, Phys. Lett. A **175**, 273–276 (1994).
37. K.-X. Sun, M.M. Fejer, E. Gustafson and R.L. Byer, Phys. Rev. Lett. **76**, 3053–3056 (1996).
38. P. Fritschel, D. Shoemaker and R. Weiss, Appl. Opt. **31**, 1412–1418 (1992).
39. L. Schnupp, Max Planck Institut für Quantenoptik, D–85748 Garching, Germany (personal communication, 1986).
40. LISA, *Pre-Phase A Report* (Max-Planck-Institut für Quantenoptik, 85748 Garching, Germany, 1995).
41. K.S. Thorne, *Probing Black Holes and Relativistic Stars with Gravitational Waves*, gr-qc-9706079 (1997).
42. J.-Y. Vinet, B.J. Meers, C.N. Man and A. Brillet, Phys. Rev. D **38**, 433–447 (1988).